Supporting Information

Synthesis of Bio-Inspired Curcuminoid Small Molecules for Solution-Processed Organic Solar Cells with High Open Circuit Voltage

Florence Archet,[†] Dandan Yao,[‡] Sylvain Chambon,[†] Mamatimin Abbas,[†] Anthony D'Aléo,[‡] Gabriel Canard,[‡] Miguel Ponce-Vargas,[§] Elena Zaborova,[‡] Boris Le Guennic,*[,§] Guillaume Wantz,*[,†] and Frédéric Fages*[,‡]

[†] Bordeaux INP, Université de Bordeaux, CNRS, IMS UMR 5218, 33400 Talence, France.

[‡] Aix Marseille Univ, CNRS, CINaM UMR 7325, 13288 Marseille Cedex 9, France.

[§] Institut des Sciences Chimiques de Rennes, UMR 6226 CNRS, Université de Rennes 1, 263 Av. du Général Leclerc, 35042 Cedex Rennes, France.

Material and methods

Synthetic procedures

Tables

Figures

Figure S4. Lippert-Mataga plots (Stokes shift vs solvent polarity parameter Δf ')

Figure S5. Cyclic voltamograms of compounds **1** - **3** (10^{-3} M) recorded in DCM (*n*-Bu_4NPF_6, 0.1 M) at 100-mV/s scan rate.

Figure S6. Top: HOMO and LUMO plots for compounds **1** - **3** (contour threshold of 0.02 a.u.); bottom: Electronic Density Difference representations. The blue (grey) regions indicate increase (decrease) of electron density upon electronic excitation (cut-off = 0.0004 a.u)

Figure S7. Comparison of *JV* curves under 100 mW/cm² illumination of BHJ OSCs made with **1** – **3**:$PC_{61}BM$ (ratio 50:50 w/w).

Figure S8. Quenching of thin-film fluorescence of **1** in $PC_{61}BM$:**1** blends versus w% of $PC_{61}BM$.

Figure S9. Tapping-mode AFM images (2 × 2 μm²) of thin films of **1**:$PC_{61}BM$ with different blend ratios: (a) 85:15, (b) 75:25, (c) 65:35 (w/w). Scales are [-2, 2 nm] for height images (top) and [-0.5, 0.5 V] for phase images (bottom).

Figure S10. UV-vis absorption spectra of compound **1** in the presence of increasing amounts of $PC_{61}BM$ (right: normalized with absorbance at 1.0). Top: in chlorobenzene; bottom: in thin films.

Figure S11. Impact of the host solvents on the EQE spectra of solution-processed BHJ OSCs based on **1**:$PC_{61}BM$ (35:65 w/w).

Figure S12. Tapping-mode AFM images (1 × 1 μm²) of thin films of 1:$PC_{61}BM$ (65 w% of $PC_{61}BM$) processed from different solvents: (a) DCB, (b) CB, (c) CF. Scales are [-1.5, 1.5 nm] for height images (top) and [-20, 20 mV] for phase images (bottom).

References

Complete lists of authors for references 3 and 11 in manuscript.

Materials and methods

Chemicals and spectroscopic characterizations. All solvents for synthesis were of analytic grade. NMR spectra (^{1}H, ^{13}C, and ^{19}F) were recorded at room temperature on a JEOL JNM ECS 400 (400, 100, and 374 MHz for ^{1}H, ^{13}C, and ^{19}F, respectively) spectrometer. Data are listed in parts per million (ppm) and are reported relative to tetramethylsilane (^{1}H and ^{13}C); residual solvent peaks of the deuterated solvents were used as internal standards. Mass spectra were obtained in Spectropole, Marseille (http://www.spectropole.fr/). Thermogravimetric analysis (TGA) was performed using a TA Instruments Q50 apparatus.

Electrochemistry. Cyclic voltammetry (CV) data were acquired using a BAS 100 Potentiostat (Bioanalytical Systems) and a PC computer containing BAS100W software (v2.3). A three-electrode system with a Pt working electrode (diameter 1.6 mm), a Pt counter electrode and a Ag/AgCl (with 3M NaCl filling solution) reference electrode was used. *n*-Bu_4NPF_6 (0.1 M in CH_2Cl_2) served as an inert electrolyte. Cyclic voltammograms were recorded at a scan rate of 100 $mV.s^{-1}$ on solution of compounds **1 - 3** at a concentration of *ca*. 10^{-3} M. Ferrocene was used as an internal standard.

Electronic absorption and fluorescence emission. UV-vis absorption measurements were carried out on a SAFAS UV mc spectrophotometer and on a Varian Cary 50. Emission spectra were obtained using a Horiba-Jobin Yvon Fluorolog-3 spectrofluorimeter equipped with a three-slit double-grating excitation and a spectrograph emission monochromator with dispersions of 2.1 $nm.mm^{-1}$ (1200 $grooves.mm^{-1}$). A 450W xenon continuous wave lamp provided excitation and fluorescence of diluted solutions was detected at right angle using 10-mm quartz cuvettes.

Computational Details

All DFT/TD-DFT calculations were carried out with the Gaussian09 program,[1] tightening self-consistent field convergence thresholds (10^{-10} a.u.) and geometry optimization (10^{-5} a.u.) convergence thresholds. For all calculations the hybrid M06-2X[2] functional has been used. All atoms were described with 6-311G(2d,p) basis sets. The solvent effects were included according to the Polarizable Continuum Model (PCM).[3] using a linear-response nonequilibrium approach for the TD-DFT step.[4,5] All HOMO-LUMO isosurfaces and EDD maps have been plotted with the Chemcraft code,[6] considering a contour threshold of 0.02 a.u. for the former and 0.0004 a.u. for the latter.

Single-crystal X-ray structure analysis. The intensity data for the single-crystal X-ray-diffraction analysis of compound **1** were collected at RT on a Bruker-Nonius Kappa CCD diffractometer by using Cu/Kα radiation (λ = 1.54184 Å). Data collection was performed with COLLECT,[7][34] cell-refinement and data-reductionwere performed with DENZO/SCALEPACK.[8] The structure was solved with SIR92 [9] and SHELXL-97 [10] was used for full-matrix least-squares refinement. Then, the H atoms were introduced at idealized positions and constrained to their parent atom during the last refinements.

OSCs fabrication. Prepaterned ITO glass substrates were subsequently cleaned by sonification in deionised (DI) water and soap, in DI water and in isopropanol, followed by a 15 min UV-ozone treatment. Then, a thin layer (≈ 45 nm) of PEDOT:PSS (Clevios PH Heraeus, filtered at

0.2 μm) was deposited by spin-coating. Substrates were baked at 120°C for 10 min to remove residual water and then were transferred into a nitrogen atmosphere glovebox. The active layer was deposited by spin-coating from 20 mg/mL solutions in chlorobenzene or chloroform and from 35 mg/mL solutions in *o*-dichlorobenzene. Spin-coating conditions were adjusted to obtain a 70-80 nm thick active layer (measured by a Detktak profilometer). Finally, a 20 nm thick layer of calcium and a 80 nm thick layer of aluminium were subsequently deposited ($P < 5.10^{-6}$ bar) through a shadow mask defining 10.5-mm² active area devices. OSCs were characterized under N_2 atmosphere using a K.H.S. SolarCelltest-575 solar simulator with HMI source and AM1.5G filters (ATLAS). The metal halide lamp was calibrated at 1000 W/m² using IL400BL radiometer.

External quantum efficiency (EQE) spectra. Prior to EQE measurements, OSC were encapsulated with epoxy glue (DELO-KATIOBOND LP655). EQE measurements were performed on a Horiba-Jobin-Yvon setup using a xenon lamp and monochromator, UV, IR filters, and silicon diode with spherical integrator for calibration of the incident light intensity.

OFET fabrication. Silicon wafers were subsequently cleaned by sonification in acetone, ethanol and DI water, followed by 15 min UV-ozone treatment. Then, a thin layer of Poly(1-vinyl-1,2,4 triazole (PVT) is deposited by spin-coating (2000 rpm, from 3 mg/mL in DI water solution). Substrates were baked in an oven at 80°C for 2 hours to remove residual water and were then transferred into a nitrogen atmosphere glovebox. **1 – 3** and **1**:$PC_{61}BM$ BHJ were deposited by spin-coating at 1000 rpm from 10 mg/mL and 20 mg/mL solutions in chlorobenzene, respectively. Then a 10 nm thick layer of MoO_x was deposed by thermal evaporation ($P < 10^{-5}$ bar), followed by a 60 nm thick layer of silver. Transfer curves of OFET were recorded in linear regime (bias ± 5 V) under N_2 atmosphere.

Atomic force microscopy. AFM measurements were carried out in tapping mode with a Bruker Innova SPM and using Olympus cantilevers (OMCL AC-160-TS). Samples were prepared on PEDOT:PSS coated substrates using the same preparation conditions described for OSC devices.

Synthetic procedures

Compound 1: 4,6-bis((E)-4-(diphenylamino)styryl)-2,2-difluoro-2H-1,3,2-dioxaborinin-1-ium-2-uide.

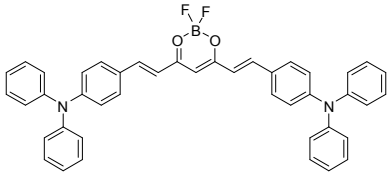

In a 50 mL flask, the mixture of 2,4-pentanedione (150 μL, 1.463 mmol, 1 eq) and $BF_3{\cdot}Et_2O$ (199 μL, 1.609 mmol, 1.1 eq) in 3 mL ethyl acetate was heated for 30min at 50-60 ^oC in air. 4-(*N*,*N*-Diphenylamino)-benzaldehyde (1 g, 3.658 mmol, 2.5 eq) and B(*n*-OBu)$_3$ (0.987 mL, 3.658 mmol, 2.5 eq) were dissolved into 12 mL ethyl acetate, and the solution was injected into the reaction mixture. After stirring for 30 min at 50-60 ^oC, a first portion of *n*-$BuNH_2$ (58μL, 0.585mmol, 0.4 eq) was added dropwise into the reaction. After 6 h heating, a second portion of *n*-$BuNH_2$ (29 μL, 0.293mmol, 0.2 eq) was added, and the reaction was kept heating at 50-60 ^oC overnight. All the solvents were evaporated. The crude product was subjected to flash column chromatography (silica, CH_2Cl_2). Purification was performed by repeating precipitation in CH_2Cl_2/petroleum ether, giving a dark green powder (700 mg, 72% yield).

^1H NMR (400 MHz, $CDCl_3$, ppm): 7.95 (d, ^3J= 15.4 Hz, 2H), 7.43 (d, ^3J= 8.8 Hz, 4H), 7.33 (m, 8H), 7.15 (m, 12H), 6.98 (d, ^3J= 8.8 Hz, 4H), 6.51 (d, ^3J= 15.4 Hz, 2H), 5.96 (s, 1H); ^{13}C NMR (400 MHz, $CDCl_3$, ppm): 178.6, 151.3, 146.4, 146.2, 130.7, 129.6, 126.7, 126.0, 124.8, 120.5, 117.3, 101.7. HRMS (ESI+) $[M + H]^+$ calcd for $C_{43}H_{34}N_2O_2BF_2^+$ m/z= 659.2681, found m/z= 659.2683.

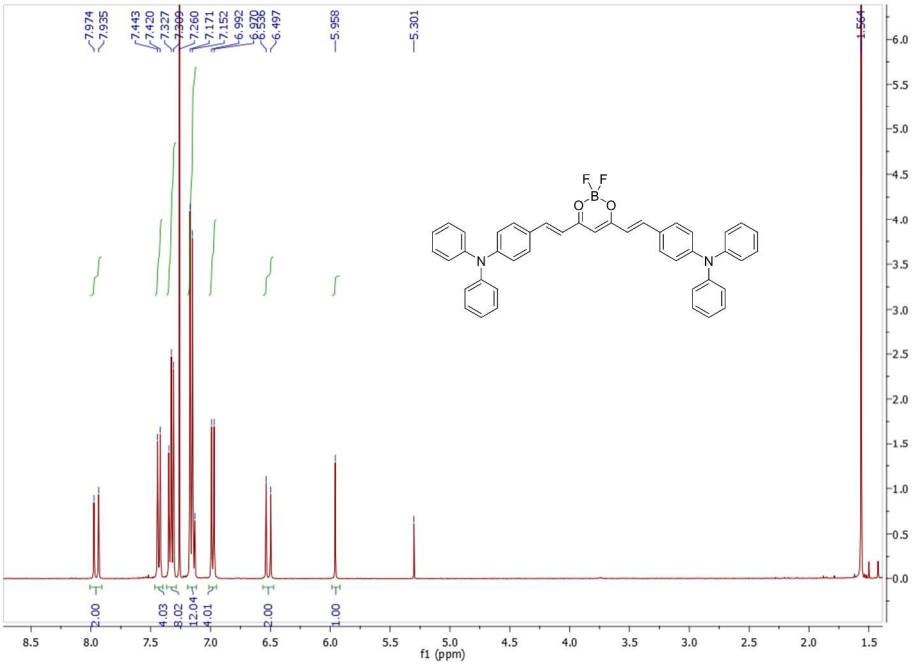

Figure NMR1. ^1H NMR spectrum of compound **1**.

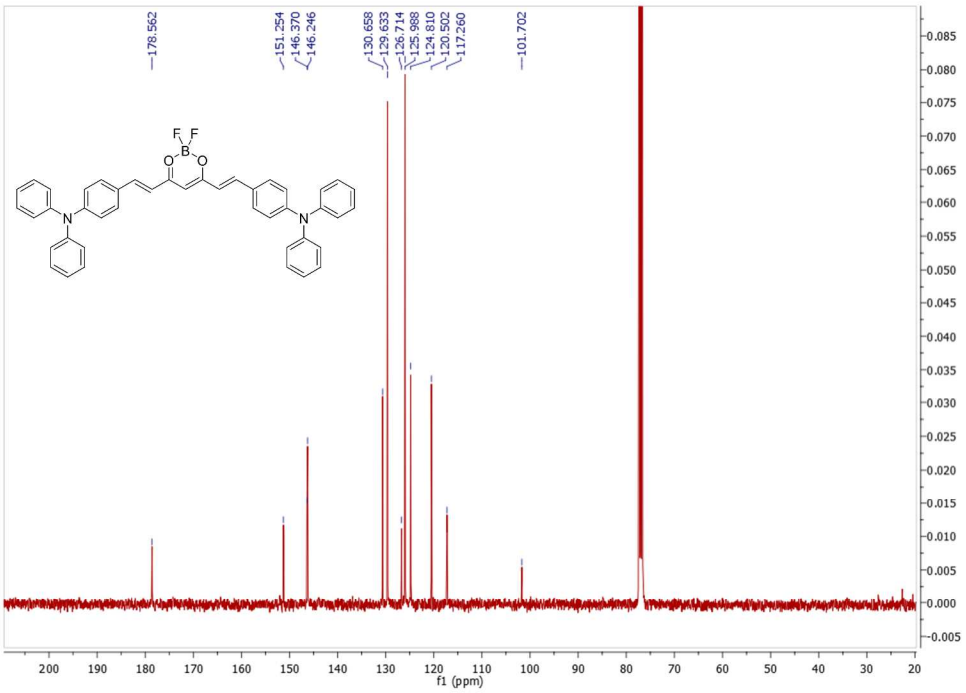

Figure NMR2. ^{13}C NMR spectrum of compound **1**.

Compound 2*:* 5-chloro-4,6-bis((E)-4-(diphenylamino)styryl)-2,2-difluoro-2H-1,3,2-dioxaborinin-1-ium-2-uide.

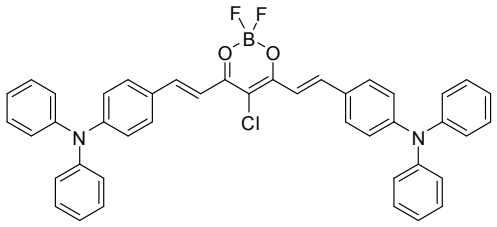

Using the same protocol as for compound **1**, compound **2** was obtained as a dark green powder (345 mg, 34% yield) using 3-chloro-2,4-pentanedione (197 mg, 1.463 mmol, 1 eq), $BF_3{\cdot}Et_2O$ (199 µL, 1.609 mmol, 1.1 eq) and 4-(*N*,*N*-diphenylamino)-benzaldehyde (1 g, 3.658 mmol, 2.5 eq). Because of the presence of the electronegative chlorine atom, the boron difluoride chelate in **2** was found less stable than that in **1** an **3**, leading to boron decoordination during purification steps. This explains the lower isolated yield.

^{1}H NMR (400 MHz, CD_2Cl_2, ppm): 8.01 (d, ^3J= 15.2 Hz, 2H), 7.53 (d, ^3J= 8.8 Hz, 4H), 7.33 (m, 4H), 7.16 (m, 14H), 6.94 (d, ^3J= 9.2 Hz, 4H); ^{13}C NMR (400 MHz, CD_2Cl_2, ppm): Not soluble enough. HRMS (ESI+) $[M + H]^+$ calcd for $C_{43}H_{33}N_2O_2BClF_2^+$ m/z= 693.2294, found m/z= 693.2296.

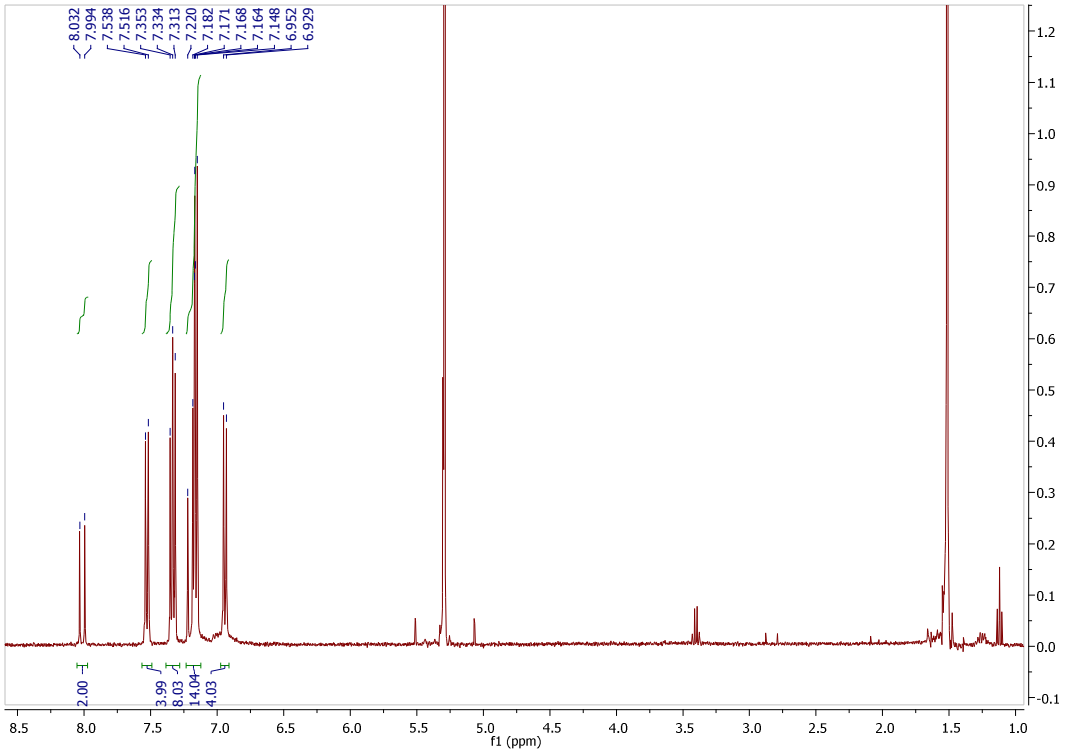

Figure NMR3. ^{1}H NMR spectrum of compoud **2**.

Compound 3. 5-Phenyl-4,6-bis((E)-4-(diphenylamino)styryl)-2,2-difluoro-2H-1,3,2-dioxaborinin-1-ium-2-uide

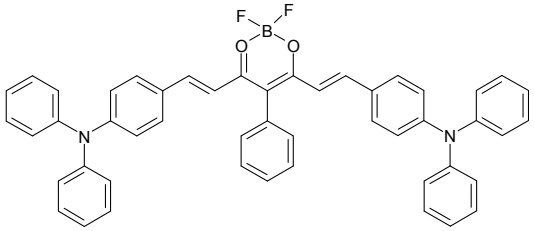

Using the same protocol as for compound **1**, compound **3** was obtained as a dark green powder (820 mg, 76% yield) using 3-phenyl-2,4-pentanedione (258 mg, 1.463 mmol, 1 eq), $BF_3{\cdot}Et_2O$ (199 µL, 1.609 mmol, 1.1 eq) and 4-(*N*,*N*-diphenylamino)-benzaldehyde (1 g, 3.658 mmol, 2.5 eq).

^{1}H NMR (400 MHz, $CDCl_3$, ppm): 8.09 (d, ^{3}J= 15.3 Hz, 2H), 7.56 (m, 4H), 7.39 (m, 12H), 7.34 (d, ^{3}J= 8.8 Hz, 4H), 7.24 (m, 10H), 7.00 (d, ^{3}J= 8.8 Hz, 4H), 6.42 (d, ^{3}J= 15.3 Hz, 2H); ^{13}C DEPT-135 NMR (400 MHz, $CDCl_3$, ppm): 146.7, 132.1, 130.8, 129.7, 129.0, 128.5, 126.0, 124.9, 120.4, 116.4. HRMS (ESI+) $[M + Na]^+$ calcd for $C_{49}H_{37}N_2O_2BF_2Na^+$ m/z= 757.2817, found m/z= 757.2824.

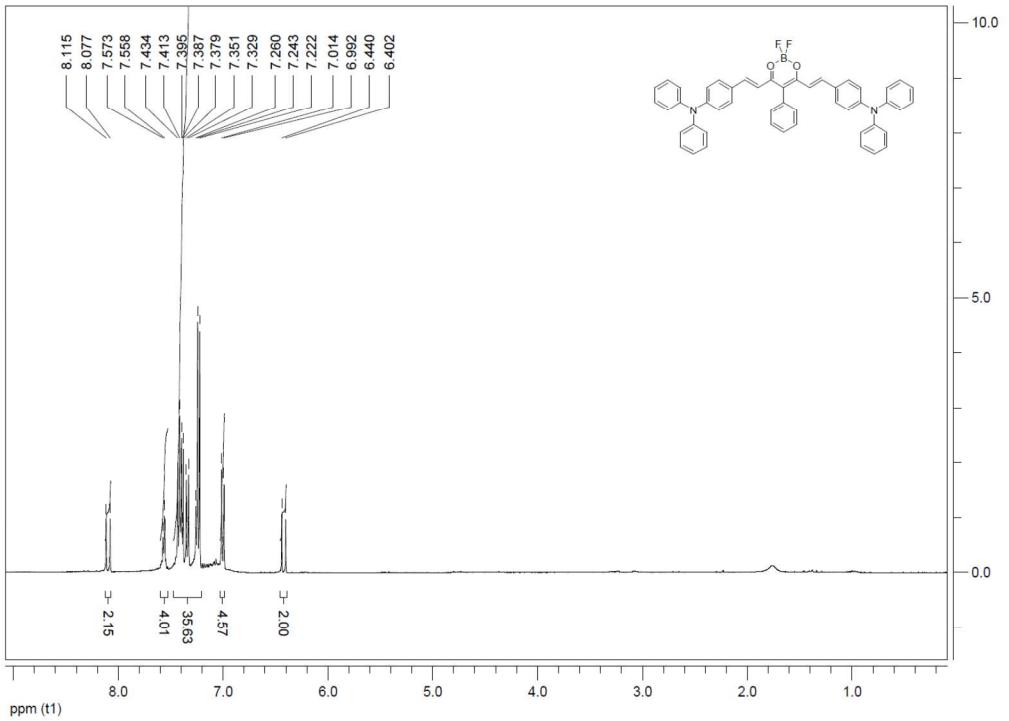

Figure NMR4. ^{1}H NMR spectrum of compoud **3.**

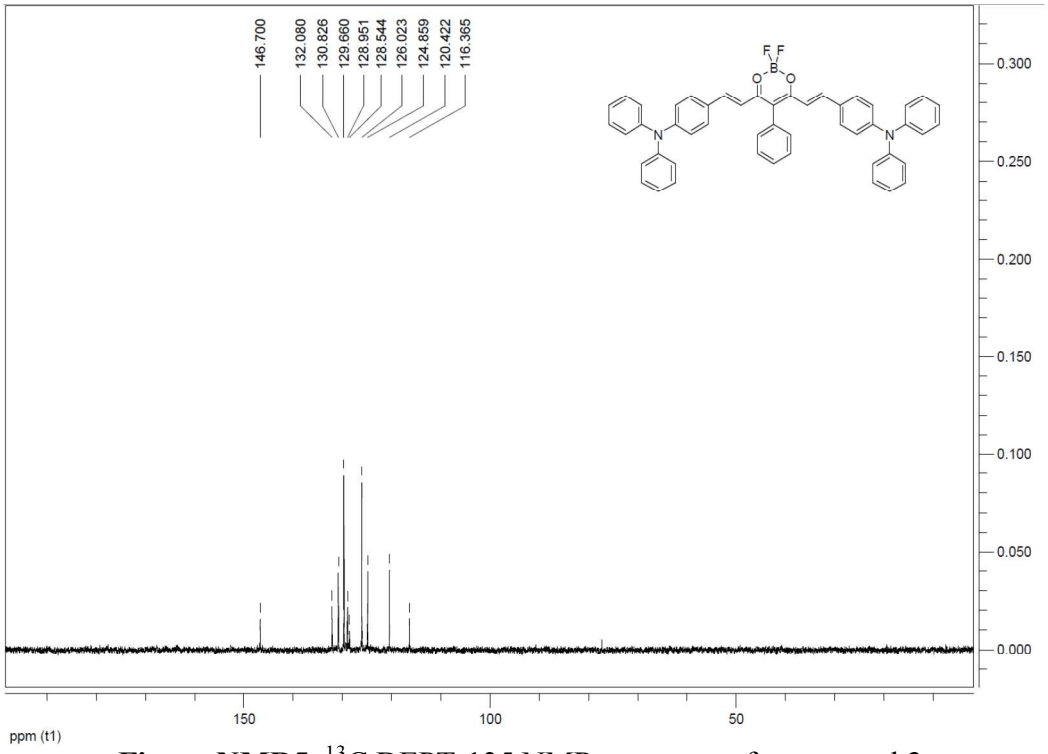

Figure NMR5. ^{13}C DEPT-135 NMR spectrum of compound **3**.

Table S1. Selected crystal data for compound **1**.

Compound **1**			
Formula	$C_{43}H_{33}BF_2N_2O_2$	Z	4
M / g/mol	658.52	λ(Cu/$K\alpha$) / Å	1.54184
Size / mm^3	0.30 × 0.2 × 0.05	T / K	293
Crystal description	plate	Dc / g.cm^{-3}	1.034
Crystal System	monoclinic	θ range / deg	min 4.2230 max 69.2320
Space group	P 2_1/n	*hkl* range	-24 / 24 -12 / 12 -19 /25
a / Å	20.0059(4)	Refln measured	30892
b / Å	10.21580(15)	Refln $I > 2\sigma(I)$	7815
c / Å	20.7995(3)	R1 $I > 2\sigma(I)$	0.0507
α / deg	90	R1 all data	0.0597
β / deg	95.6846(16)	*w*R2 $I > 2\sigma$(I)	0.1424
γ / deg	90	*w*R2 all data	0.1504
V / Å^3	4230.03(12)	$\Delta\rho$ (+/-) / e. Å^{-3}	min -0.365 max 0.326

Table S2. Electrochemical[a] and optical[b] data for compound **1** - **3**.

Compound	E_{red} (V)	E_{ox} (V)	E_{red}^{onset} (V)	E_{ox}^{onset} (V)	HOMO[c] (eV)	LUMO[c] (eV)	E_g^{el} (eV)	E_g^{op} (eV)	λ_{abs}^{onset} (nm)
1	-1.27	+0.58	-1.19	+0.50	-5.65	-3.96	1.69	1.75	710
2	-1.09	+0.60	-1.04	+0.52	-5.67	-4.11	1.56	1.64	756
3	-1.25	+ 0.57	-1.18	+0.45	-5.60	-3.97	1.63	1.75	710

[a] Measured in DCM containing 0.1 M of (n-Bu)$_4$NPF$_6$ using a scan rate of 100 mV/s. Ferrocene (Fc) was used as an internal standard. Redox potential values are given against Fc/Fc$^+$. [b] Optical band gap obtained from the onset of the thin-film electronic absorption spectrum. [c] Energies of HOMO and LUMO levels were obtained using HOMO = -|el(E_{ox}^{onset} + 5.15) eV and LUMO = -|el(E_{red}^{onset} + 5.15) eV.

Table S3. Theoretical vertical electronic absorption data obtained for compounds **1** - **3** in CH_2Cl_2 solution.

Compound		λ_{max} (nm)	λ_{max} (cm^{-1})	f [a]	Assignment (%)	
1	I	500	20000	2.637	HOMO→LUMO	(83.97)
	II	283	35336	0.292	HOMO→LUMO+5 HOMO-1→LUMO+4	(36.15) (35.39)
	III	287	34843	0.190	HOMO-1→LUMO+1	(55.70)
	IV	283	35335	0.160	HOMO-1→LUMO+5 HOMO→LUMO+4	(36.26) (35.15)
	V	410	24390	0.160	HOMO-1→LUMO	(86.39)
2	I	527	18975	2.654	HOMO→LUMO	(83.98)
	II	281	35587	0.225	HOMO-1→LUMO+4 HOMO→LUMO+5	(29.49) (20.43)
	III	292	34247	0.197	HOMO-1→LUMO+1	(57.75)
	IV	281	35587	0.190	HOMO-1→LUMO+5 HOMO→LUMO+5	(30.25) (27.08)
	V	424	23585	0.113	HOMO-1→LUMO	(86.60)
3	I	510	19608	2.611	HOMO→LUMO	(84.20)
	II	283	35335	0.280	HOMO→LUMO+5 HOMO-1→LUMO+4	(33.31) (24.20)
	III	288	34722	0.248	HOMO-1→LUMO+1	(53.63)
	IV	283	35335	0.152	HOMO-1→LUMO+5 HOMO→LUMO+4	(29.47) (27.26)
	V	417	23981	0.079	HOMO-1→LUMO	(85.84)

[a] Oscillator strength

Table S4. Calculated dipole moments (values in Debye) for compounds **1** – **3**.

	1	**2**	**3**
Ground state	10.700	8.805	10.887
Excited state	12.311	10.234	12.122

Table S5. Performance parameters of BHJ OSCs based on compounds **1 - 3** and $PC_{61}BM$ (blend ratio 50:50 w/w) [a].

Compound	d [b] (nm)	J_{SC} (mA/cm²)	V_{OC} (V)	FF	PCE (%)
1	79	9.02 ± 0.13	0.80 ± 0.07	0.32 ± 0.03	2.33 ± 0.39 (3.07)
2	81	4.41 ± 0.21	0.66 ± 0.04	0.28 ± 0.01	0.82 ± 0.05 (0.89)
3	91	4.61 ± 0.27	0.75 ± 0.05	0.28 ± 0.01	0.97 ± 0.01 (1.11)

[a] BHJ OSCs fabricated using the following architecture: ITO/PEDOT:PSS/**1 - 3**:$PC_{61}BM$/Ca/Al and tested under 100 mW/cm² illumination. The brackets in the PCE indicate the highest values. [b] Film thickness.

Table S6. Mobility[a] of compounds **1 - 3**.

Compound	Ratio $PC_{61}BM$:**1 – 3** (w/w)	μ_h (cm²/V.s)	μ_e (cm²/V.s)
1	0/100	$2.6.10^{-5}$	-
	65/35	$5.5.10^{-6}$	$1.5.10^{-4}$
2	0/100	$4.6.10^{-6}$	-
3	0/100	$< 10^{-6}$	-

[a] Measured from OFET.

Table S7. Impact of the blend ratio on performances parameters of BHJ OSCs based on compound **1** and $PC_{61}BM$[a].

Ratio $PC_{61}BM$:**1** (w/w)	d[b] (nm)	J_{SC} (mA/cm²)	V_{OC} (V)	FF	PCE (%)
15/85	78	3.54 ± 0.10	0.92 ± 0.10	0.27 ± 0.01	0.92 ± 0.08 (1.00)
25/75	80	4.45 ± 0.06	0.92 ± 0.09	0.27 ± 0.01	1.18 ± 0.13 (1.30)
30/70	85	6.32 ± 0.24	0.81 ± 0.09	0.30 ± 0.02	1.51 ± 0.16 (1.73)
35/65	78	7.28 ± 0.23	0.83 ± 0.09	0.30 ± 0.02	1.86 ± 0.34 (2.30)
40/60	78	7.78 ± 0.10	0.84 ± 0.10	0.32 ± 0.03	2.12 ± 0.37 (2.67)
45/55	74	8.58 ± 0.10	0.83 ± 0.07	0.33 ± 0.02	2.35 ± 0.28 (2.74)
50/50	80	9.02 ± 0.13	0.80 ± 0.07	0.32 ± 0.03	2.33 ± 0.39 (3.07)
55/45	76	9.28 ± 0.08	0.86 ± 0.06	0.36 ± 0.02	2.86 ± 0.40 (3.52)
60/40	74	9.41 ± 0.26	0.81 ± 0.06	0.35 ± 0.02	2.66 ± 0.37 (3.26)
65/35	73	9.30 ± 0.20	0.83 ± 0.05	0.35 ± 0.02	2.72 ± 0.32 (3.22)
70/30	72	9.23 ± 0.10	0.79 ± 0.04	0.35 ± 0.02	2.52 ± 0.24 (2.94)
75/25	74	8.41 ± 0.43	0.63 ± 0.05	0.31 ± 0.01	1.70 ± 0.22 (1.95)
85/15	75	6.50 ± 0.11	0.59 ± 0.03	0.30 ± 0.01	1.20 ± 0.09 (1.28)

[a] BHJ OSCs fabricated using the following architecture: ITO/PEDOT:PSS/**1**:$PC_{61}BM$/Ca/Al and tested under 100 mW/cm² illumination. The brackets in the PCE indicate the highest values. [b] Film thickness.

Table S8. Impact of the host solvents on the performance of solution-processed BHJ OSCs based on **1**:$PC_{61}BM$ (35:65 w/w)[a].

	d[b] (nm)	J_{SC} (mA/cm²)	V_{OC} (V)	FF	PCE (%)
CF	73	9.50 ± 0.29	0.950 ±0.037	0.381 ± 0.019	3.45 ± 0.32 (4.14)
CB	70	9.30 ± 0.20	0.83 ± 0.05	0.35 ± 0.02	2.72 ± 0.32 (3.22)
DCB	62	9.02 ± 0.05	0.839 ± 0.028	0.352 ± 0.017	2.67 ± 0.19 (2.66)

[a] BHJ OSCs fabricated using the following architecture: ITO/PEDOT:PSS/**1**:$PC_{61}BM$/Ca/Al and tested under 100 mW/cm² illumination. The brackets in the PCE indicate the highest values. [b] film thickness.

Figure S1. TGA of **1** recorded at 10 °C/min.

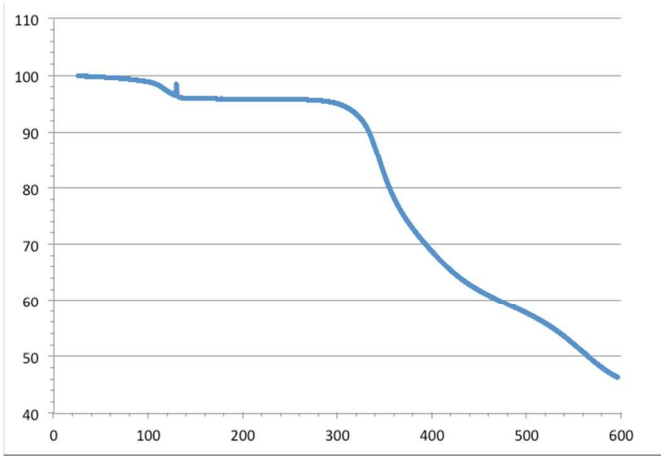

Figure S2. Single-crystal X-ray analysis of compound **1**. Left: spatial arrangement of **1** in the crystal lattice; right**:** π-stack of **1** along *b* axis (for clarity hydrogen atoms are omitted).

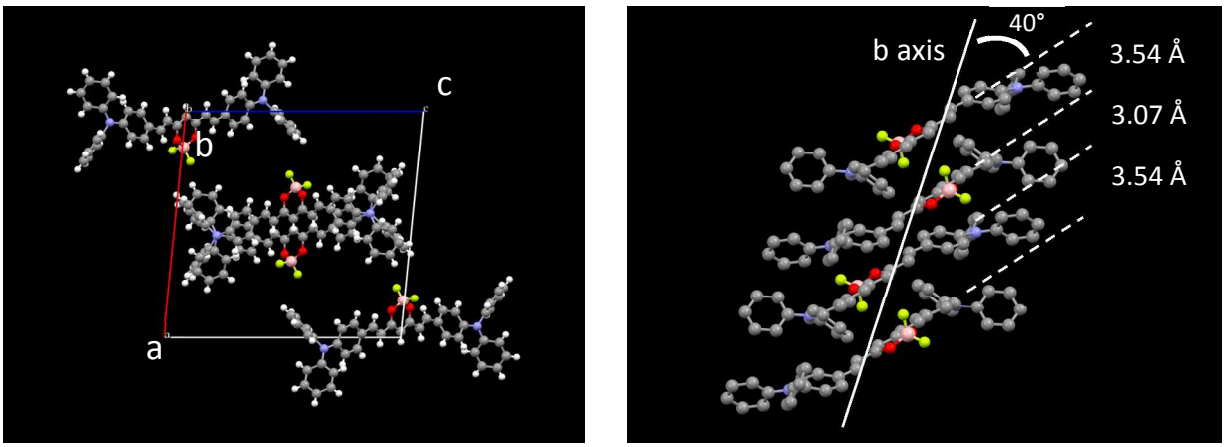

Figure S3. UV-vis absorption (left) and fluorescence emission (right) spectra of **1** and **2** in solvents of different polarities.

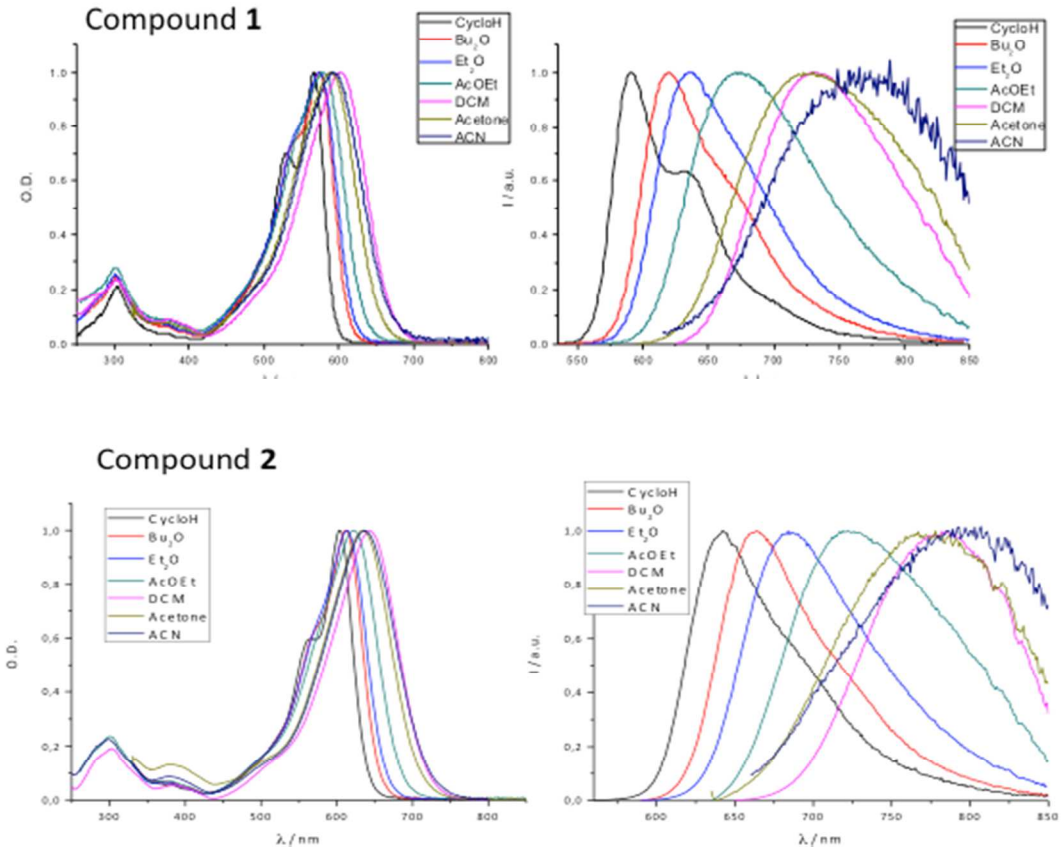

Figure S4. Lippert-Mataga plots: Stokes shift *vs.* solvent polarity function Δf ' (Δf ' = [(ε - 1)/(2ε + 1)] – 0.5 [(n^2 - 1)/(2n^2 + 1)])

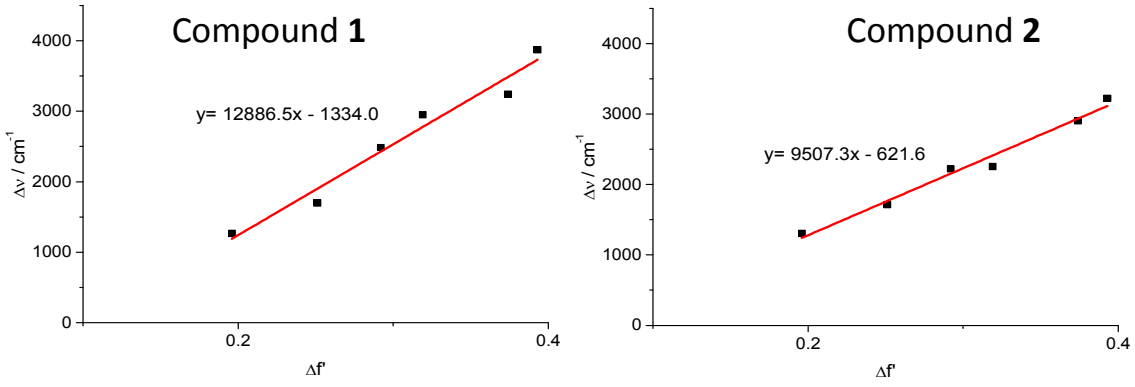

Figure S5. CVs of compounds **1** - **3** (10^{-3} M) recorded in DCM (*n*-Bu_4NPF_6, 0.1 M) at 100-mV/s scan rate.

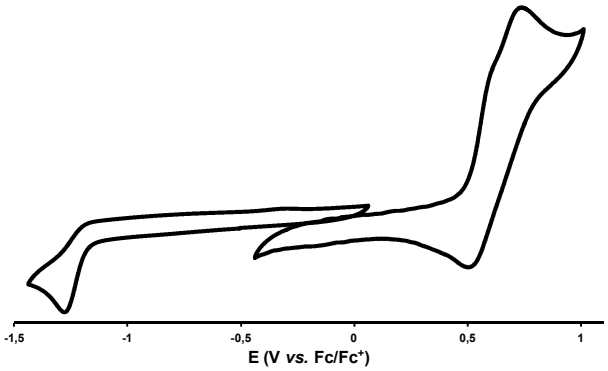

Compound **1**

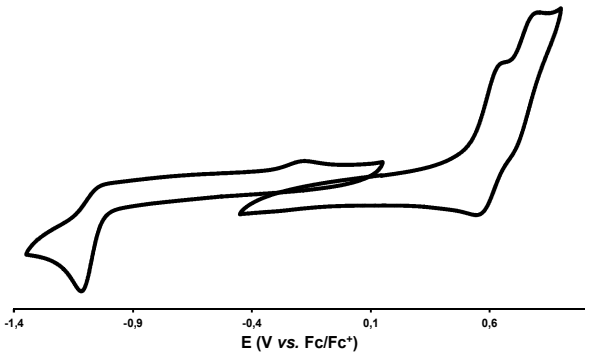

Compound **2**

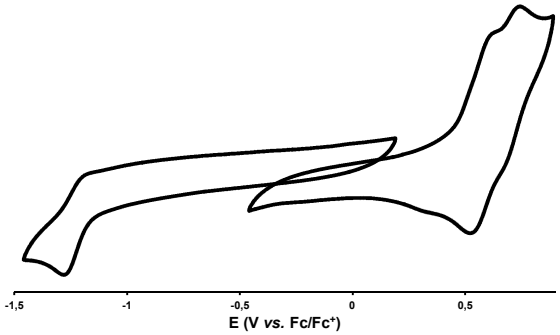

Compound **3**

Figure S6. Top: HOMO and LUMO plots for compounds **1** - **3** (contour threshold of 0.02 a.u.); bottom: Electronic Density Difference representations. The blue (grey) regions indicate increase (decrease) of electron density upon electronic excitation (cut-off = 0.0004 a.u.)

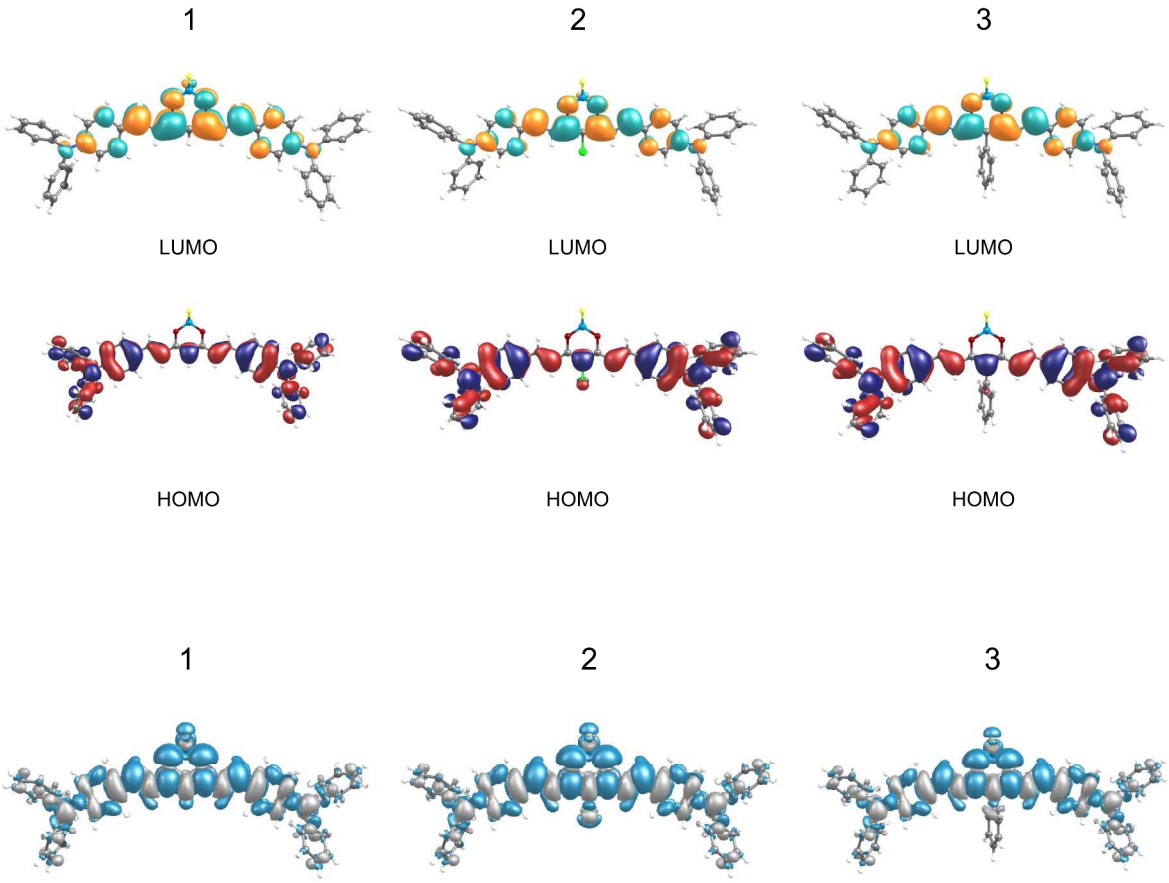

Figure S7. Comparison of *JV* curves under 100 mW/cm² illumination of BHJ OSCs made with **1 – 3**:$PC_{61}BM$ (ratio 50:50 w/w).

Figure S8. Quenching of thin-film fluorescence of **1** in $PC_{61}BM$:**1** blends versus w% of $PC_{61}BM$.

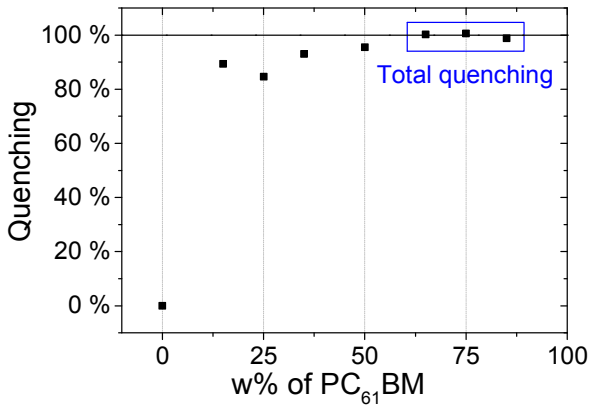

Figure S9. Tapping-mode AFM images (2 × 2 μm²) of thin films of **1**:$PC_{61}BM$ with different blend ratios: (a) 85:15, (b) 75:25, (c) 65:35 (w/w). Scales are [-2, 2 nm] for height images (top) and [-0.5, 0.5 V] for phase images (bottom).

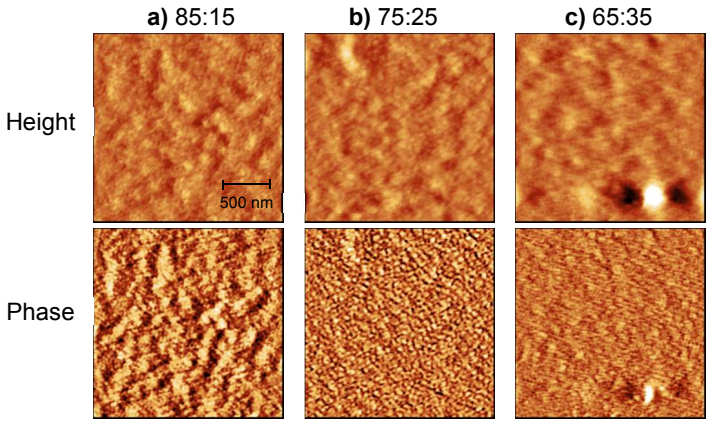

Figure S10. UV-vis absorption spectra of compound **1** in the presence of increasing amounts of $PC_{61}BM$ (right: normalized with absorbance at 1.0). Top: in chlorobenzene; bottom: in thin films.

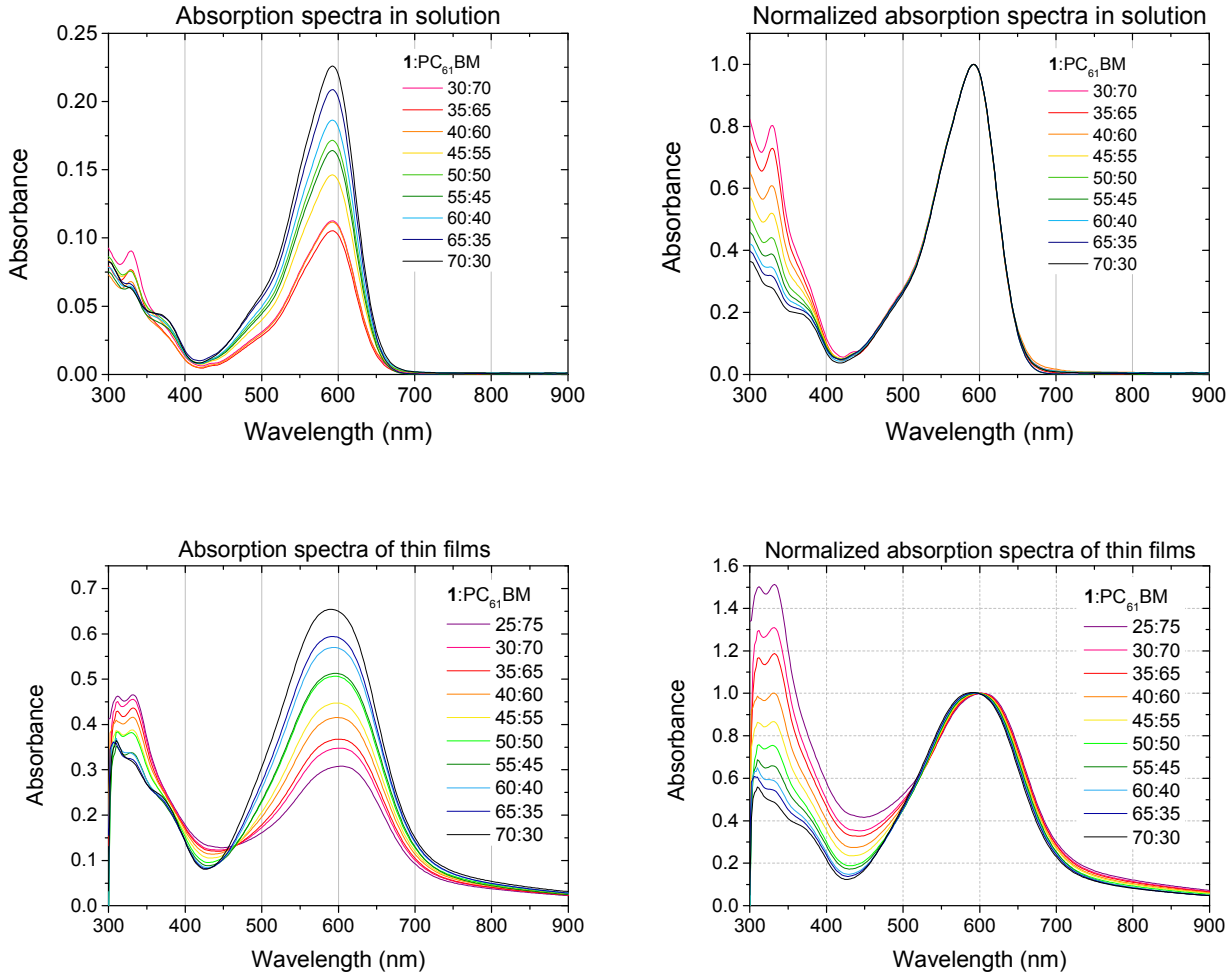

Figure S11. Impact of the host solvents on the EQE spectra of solution-processed BHJ OSCs based on **1**:$PC_{61}BM$ (35:65 w/w).

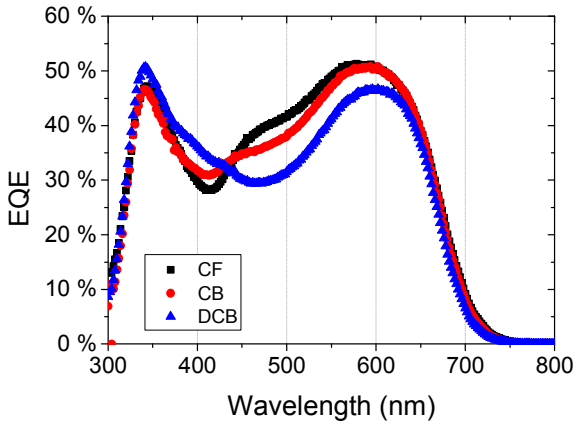

Figure S12. Tapping-mode AFM images (1 × 1 μm²) of thin films of **1**:$PC_{61}BM$ (65 w% of $PC_{61}BM$) processed from different solvents: (a) DCB, (b) CB, (c) CF. Scales are [-1.5, 1.5 nm] for height images (top) and [-20, 20 mV] for phase images (bottom).

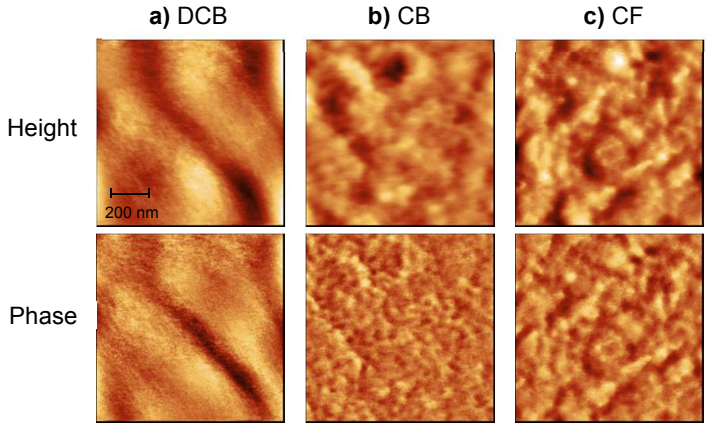

References

1) Gaussian 09. Revision D. 01. Gaussian 09, Revision D.01, M. J. Frisch, G. W. Trucks, H. B. Schlegel, G. E. Scuseria, M. A. Robb, J. R. Cheeseman, G. Scalmani, V. Barone, G. A. Petersson, H. Nakatsuji, X. Li, M. Caricato, A. Marenich, J. Bloino, B. G. Janesko, R. Gomperts, B. Mennucci, H. P. Hratchian, J. V. Ortiz, A. F. Izmaylov, J. L. Sonnenberg, D. Williams-Young, F. Ding, F. Lipparini, F. Egidi, J. Goings, B. Peng, A. Petrone, T. Henderson, D. Ranasinghe, V. G. Zakrzewski, J. Gao, N. Rega, G. Zheng, W. Liang, M. Hada, M. Ehara, K. Toyota, R. Fukuda, J. Hasegawa, M. Ishida, T. Nakajima, Y. Honda, O. Kitao, H. Nakai, T. Vreven, K. Throssell, J. A. Montgomery, Jr., J. E. Peralta, F. Ogliaro, M. Bearpark, J. J. Heyd, E. Brothers, K. N. Kudin, V. N. Staroverov, T. Keith, R. Kobayashi, J. Normand, K. Raghavachari, A. Rendell, J. C. Burant, S. S. Iyengar, J. Tomasi, M. Cossi, J. M. Millam, M. Klene, C. Adamo, R. Cammi, J. W. Ochterski, R. L. Martin, K. Morokuma, O. Farkas, J. B. Foresman, and D. J. Fox, Gaussian, Inc., Wallingford CT, 2016.Gaussian. Inc., Wallingford CT, **2009**.
2) Zhao, Y.; Truhlar, G. *Theor. Chem. Acc*. **2008**, *120*, 215-241.
3) Tomasi, J.; Mennucci, B.; Cammi, R. *Chem. Rev*. **2005**, *105*, 2999-3093.
4) Cossi, M.; Barone, V. *J. Chem. Phys*. **2001**, *115*, 4708–4717.
5) Improta, R.; Barone, V.; Scalmani, G.; Frisch, M. J. *J. Chem. Phys*. **2006**, *125*, 054103.
6) Andrienko, G. http://www.chemcraftprog.com.
7) COLLECT, Nonius BV, Delft, The Netherlands, **2001**.

8) Otwinowski, Z.; Minor, W. *Methods in Enzymology, in Macromolecular Crystallography*, Part A, Vol. 276 (Eds.: C. W. Carter, Jr., R. M. Sweet), Academic Press, New York, **1997**, pp. 307 –326.

9) Altomare, A.; Cascarano, G.; Giacovazzo, G.; Guagliardi, A.; Burla, M. C.; Polidori, G.; Camalli, M. *J. Appl. Crystallogr*. **1994**, *27*, 435.

10) Sheldrick, G. M. *Acta Crystallogr. A* **2008**, *64*, 112 – 122.

Complete lists of authors for references 3 and 11 in manuscript.

(3) Kan, B.; Li, M.; Liu, F.; Wan, X.; Yunchuang, W.; Wang, N.; Long, G.; Yang, X.; Feng, H.; Zuo, Y.; Zhang, M.; Huang, F.; Cao, Y.; Russell, T. P.; Chen, Y. A Series of Simple Oligomer-like Small Molecules Based on Oligothiophenes for Solution-Processed Solar Cells with High Efficiency. *J. Am. Chem. Soc.* **2015**, 137, 3886-3893.

(11) Wessendorf, C. D.; Schulz, G. L.; Mishra, A.; Kar, P.; Ata, I.; Weidelener, M.; Urdanpilleta, M.; Hanisch, J.; Mena-Osteritz, E.; Lindén, M.; Ahlswede, E.; Bäuerle, P. Efficiency Improvement of Solution-Processed Dithienopyrrole-Based A-D-A Oligothiophene Bulk-Heterojunction Solar Cells by Solvent Vapor Annealing. *Adv. Energy Mater*. **2014**, *4*, 1400266.